ACS APPLIED MATERIALS & INTERFACES

Research Article

www.acsami.org

Graphene Anodes and Cathodes: Tuning the Work Function of Graphene by Nearly 2 eV with an Aqueous Intercalation Process

Jan-Kai Chang,[†] Wei-Hsiang Lin,[†] Jieh-I Taur,[†] Ting-Hao Chen,[†] Guo-Kai Liao,[†] Tun-Wen Pi,[‡] Mei-Hsin Chen,[*,§] and Chih-I Wu[*,†]

[†]Graduate Institute of Photonics and Optoelectronics and Department of Electrical Engineering, National Taiwan University, Taipei 106, Taiwan (R.O.C.)

[‡]National Synchrotron Radiation Research Center, Hsinchu 307, Taiwan (R.O.C.)

[§]Department of Optoelectronic Engineering, National Dong Hwa University, Hualien 974, Taiwan (R.O.C.)

Supporting Information

ABSTRACT: To expand the applications of graphene in optoelectronics and microelectronics, simple and effective doping processes need to be developed. In this paper, we demonstrate an aqueous process that can simultaneously transfer chemical vapor deposition grown graphene from Cu to other substrates and produce stacked graphene/dopant intercalation films with tunable work functions, which differs significantly from conventional doping methods using vacuum evaporation or spin-coating processes. The work function of graphene layers can be tuned from 3.25 to 5.10 eV, which practically covers the wide range of the anode and cathode applications. Doped graphene films in intercalation structures also exhibit excellent transparency and low resistance. The polymer-based solar cells with either low work function graphene as cathodes or high work function graphene as anodes are demonstrated.

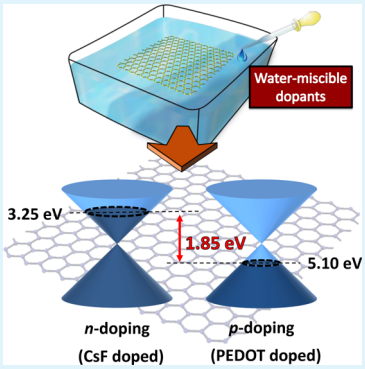

KEYWORDS: *graphene, doping, polymer-free transfer, photoemission spectroscopy, solar cell*

INTRODUCTION

Due to the superior optical, electrical, and mechanical properties within the two-dimensional monolayer of sp^2-bonded carbon atoms, graphene has been recognized as a next-generation substitute for transparent, conducting, and multifunctional electrodes in optoelectronic devices[1−4] and has attracted a great deal research devoted in recent years.[5,6] The integration of graphene with optoelectronic devices, such as light-emitting diodes, photosensors, and transparent thin film transistors, has led to the need for processes that enable tailored transfers of high-quality graphene grown by chemical vapor deposition (CVD) to desired targets.[6−15] One of the important applications of graphene is to replace the predominant tin-doped indium oxide (ITO), which would be restricted in the future due to limited indium resources. However, of many methods reported for the transfer of graphene to date, including thermal release tape, poly(methyl methacrylate)-assisted (PMMA-assisted) and their variants with a polymer carrier, suffer from degraded physical properties accompanied by residual polymer impurity during the process, which limits their application to high performance graphene based devices.[16−18] In addition, for applications such as transparent electrodes, tuning the work function of graphene is essential since the mismatch of the energy levels between the graphene electrode and materials in the active layers would degrade the performance of devices. Significant efforts have been invested to increase the work function of graphene with acid or metal doping, which enables graphene for anode applications.[5,6,19−28] On the other hand, there are few reports on optoelectronic devices using graphene as the cathodes owing to the lack of an n-doped method (with work function less than 4 eV). In this paper, we demonstrate an aqueous process that can simultaneously transfer CVD grown graphene from Cu to other substrates and produce stacked graphene/dopant intercalation films with tunable work functions for both anode and cathode application. The work function of the graphene, measured via ultraviolet spectroscopy (UPS), can be tuned from 3.25 to 5.10 eV through incorporation of various aqueous solutions. These doped graphene multilayers exhibit excellent transmittance and high sheet conductivity as transparent conductors on arbitrary substrates. Applying this method, organic solar cells with graphene as both anode and cathode were successfully demonstrated, with power conversion efficiency (PCE) of ∼3.10% using conventional poly(3-hexylthiophene)/phenyl-C61-butyric acid methyl ester (P3HT/PCBM) based bulk-heterojunction (BHJ) structures.

Received: May 7, 2015
Accepted: July 17, 2015
Published: July 17, 2015

DOI: 10.1021/acsami.5b03934
ACS Appl. Mater. Interfaces 2015, 7, 17155−17161

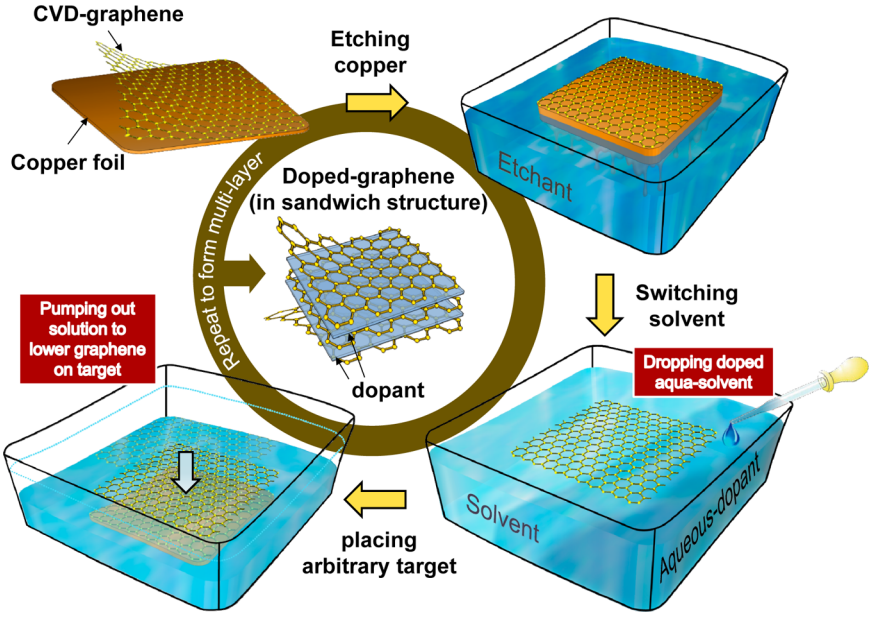

Figure 1. Schematic illustration of aqueous transfer and doping process for intercalated graphene/dopant layers.

RESULTS

Aqueous Transfer and Doping Process. The common methods for transferring graphene onto a target substrate with a polymer handle layer usually cause structural disorder and impurity contamination in the graphene films.[29,30] To create the multilayer graphene films, the repeated stacking process involves mechanical strain, solvent treatment, and residue issues, which unavoidably deteriorate the quality of the graphene sheet. Moreover, the hydrophobic character of graphene is unfavorable for conventional doping methods such as spin-coating and dip-coating.[5,31] A simple and effective doping method therefore needs to be established as a necessity for extending the application of graphene electrodes in flexible optoelectronics. A polymer-free process for transferring a large-area CVD grown graphene monolayer from copper foil to other substrates has been demonstrated by modifying the surface tension of the aqueous solution.[32] Here, we demonstrate that graphene transfer and doping processes can be achieved simultaneously with aqueous solution. Figure 1 shows the aqueous transfer/doping process to fabricate a stacking structure of graphene/dopant/graphene intercalation film. First, the as-grown CVD graphene on copper foil was placed in an ammonium persulfate solution to remove copper. After the copper layer was thoroughly etched, an aqueous solvent with isopropyl alcohol (IPA) and deionized (DI) water was gradually substituted for the etchant to sustain the floating graphene thin film. To obtain a complete piece of flawless graphene monolayer floated on the aqueous solution, a small amount of IPA was mixed in the DI water to balance the surface tension and the physical strength of the bonded carbon atoms within the graphene. The doping process was then implemented by using a syringe to inject another doped aqueous solution, which is composed of dopants such as cesium carbonate (Cs_2CO_3), cesium fluoride (CsF), polyethylenimine ethoxylated (PEIE), and poly(3,4-ethylenedioxythiophene) (PEDOT) poly(styrenesulfonate) (PSS). After the dopants were fully mixed with the aqueous solution, a target substrate was placed in the solution underneath the floating graphene thin film followed by the extraction of solution to make the doped graphene monolayer land the target substrate. In this way, the decoration of the graphene monolayer with dopant can be achieved with various work functions. To obtain the intercalated graphene stacked film, the aforementioned method was repeated with another CVD graphene/copper foil immersed into the aqueous solution. Therefore, this in situ doping process, along with the polymer-free transfer, can generate the graphene/dopant intercalated multilayer with the desired work function and improved sheet conductivity for electrode applications.

Electronic Structure of Doped Graphene Films. For p-type doping, we incorporated conducting PEDOT:PSS (high-conductivity grade PH1000), which is a conjugated polymer with hole preferential conductivity. On the other hand, two typical alkali metal salts, Cs_2CO_3 and CsF, and a novel surface modifier, PEIE, were used for n-type doping.[33] The degree of dopant protonation was further characterized by high-resolution synchrotron-radiation photoemission spectroscopy, as shown in Figure 2. The spectra featured a pronounced carbon 1s core level peak resulting from graphene layers around a binding energy of 284.5 eV with respect to the Fermi level (E_F). By comparing the core-level intensity of corresponding atoms in the dopant molecules from photoemission spectra, the doping ratio is 2.7% sulfur for PEDOT-doped graphene, 2.8% nitrogen for PEIE-doped graphene, 3.7% cesium for Cs_2CO_3-doped graphene, and 3.3% cesium for CsF-doped graphene. The presence of dopant elements in doped graphene films indicates the effective doping in graphene and suggests that the dopant molecules can be intercalated into graphene layers by liquid phase diffusion in this doping scheme even though the surface wettability of the graphene is normally poor. This differs significantly from conventional doping methods which need to address the initial hydrophobic issue of graphene to enable efficient doping.[34,35]

To better understand the doping effect in graphene films, the Fermi level variation (ΔE_F) was investigated from the evolution of the carbon 1s core level and valence band via X-ray photoemission spectroscopy (XPS) and ultraviolet photoemission spectroscopy (UPS) measurements, respectively. As

DOI: 10.1021/acsami.5b03934
ACS Appl. Mater. Interfaces 2015, 7, 17155−17161

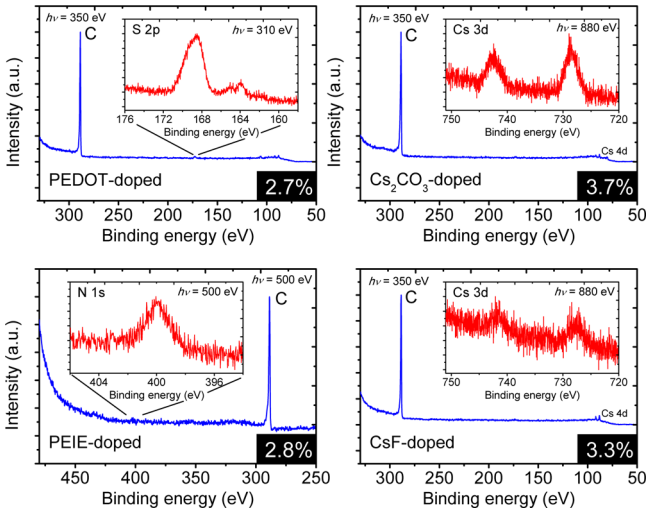

Figure 2. XPS spectra of the graphene doped with PEDOT, PEIE, Cs_2CO_3, and CsF. The effective doping ratios of dopant to graphene are 2.7% (for G:PEDOT), 2.8% (for G:PEIE), 3.7% (for G:Cs_2CO_3), and 3.3% (for G:CsF).

shown in Figure 3, the carbon 1s core level is located at the binding energy of 284.5 eV for pristine graphene (denoted as G) while the peak position varies from 283.9 to 285.7 eV for doped graphene films. Since all the binding energies in the spectra are with respect to the Fermi level, this suggests that the Fermi energies in these films are different due to the extrinsic doping. It should be noted that the shape of the carbon 1s peak was broadened slightly for PEDOT-, PEIE-, and Cs_2CO_3-doped graphene (denoted as G:PEDOT, G:PEIE, and G:Cs_2CO_3, respectively) due to the foreign molecules surrounding carbon atoms. Furthermore, the work functions were measured with UPS, determined by the shift in the secondary electron cutoff in the spectra. The pristine graphene possesses a work function of 4.50 eV which is consistent with the previous report.[32] In comparison, the work function can be modified to 5.10 eV for PEDOT-doped graphene (G:PEDOT), which is p-type as compared to pristine graphene. On the other hand, the work function of graphene can be tuned to as low as 3.25 eV by incorporating CsF (G:CsF) as the n-type dopants. The valence-band spectra on the right-hand side of Figure 3 including a distinct graphene feature near the Fermi level also underwent a similar shift.[32,36] The fact that the shift of the secondary electron cutoff in onset spectra approximates the value of shift in the carbon 1s core level as well as that in the valence-band spectra indicates that the graphene films are p-doped with PEDOT and n-doped with PEIE, Cs_2CO_3, and CsF. It should be noted that the valence-band spectra of the doped graphenes are similar to that of pristine graphene, indicating the integrity of the graphene structures after incorporation of the dopant molecules. In contrast to the work function variation induced by the interfacial dipole that can only shift the secondary electron cutoff, the simultaneous shifts of valence band and core level in reference to the Fermi level verify that the change of work function was regulated by the excess occupation or deficiency of the electron introduced by the doped molecules which alter the electronic configuration to reposition the E_F. The tunable work functions for graphene are shown in Figure 4, revealing an n-doped film with low work functions of 3.25 eV for G:CsF, 3.70 eV for G:Cs_2CO_3, and 4.20 eV for G:PEIE, and a p-doped film with a high work function of 5.10 eV for G:PEDOT. Since the doping process does not significantly depress the 2p π state in the valence-band structure, the preserved mobile π-electrons enable optimum sheet conductivity for doped graphene.

Optical and Electrical Properties. We further investigated the transmittance and sheet resistivity for doped graphene since they are the key factors for applications in optoelectronics and microelectronics. In Figure 5 the transmittance as a function of optical wavelength for various doped graphene layers on glass substrates is shown, where the insets summarize the transmittance in various stacking structures at visible wavelengths (400, 500, 600, and 700 nm). In each case, the transmittance show only slight decreases as compared to the pristine graphene,[32] with around 90% in the trilayer structure. The transmittance spectra are fading at long wavelengths (>600 nm) for G:PEDOT, especially in multilayer structures, since PEDOT possesses a higher reflection in the infrared range.[37] The n-doped graphenes with CsF, Cs_2CO_3, and PEIE show no decrease in transmittance spectra at long wavelengths. Figure 6 illustrates the sheet resistance of the doped graphene films from one to three layers, which drops as the number of graphene layers reduces. Although the single layers of graphene doped with different materials exhibit quite different conductivity, the sheet resistance of the graphene films converges to less than 300 Ω sq^{-1} after stacking three layers intercalated with these materials.

BHJ Solar Cells with Doped Graphene Electrodes. The low and high work function graphene layers were then integrated as both cathodes and anodes in organic solar cells (OSCs), respectively. The bulk heterojunction (BHJ) OSC

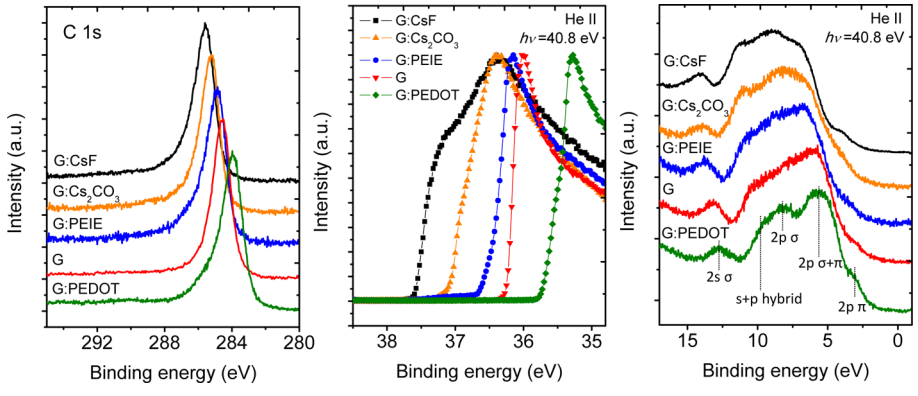

Figure 3. Carbon 1s core level and UPS spectra for G:PEDOT, G:PEIE, G:Cs_2CO_3, and G:CsF.

DOI: 10.1021/acsami.5b03934
ACS Appl. Mater. Interfaces 2015, 7, 17155−17161

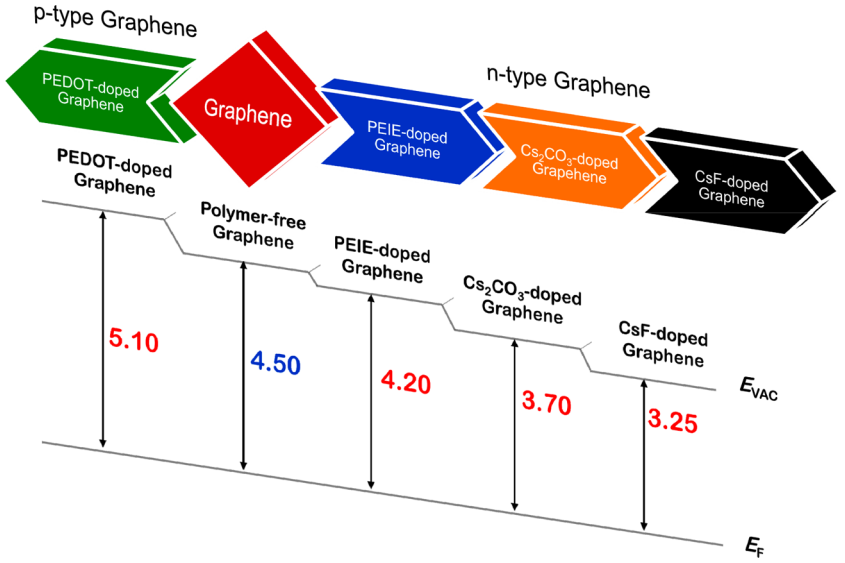

Figure 4. Schematic illustration of experimentally obtained work functions for G:PEDOT (5.10 eV), pristine graphene (4.5 eV), G:PEIE (4.20 eV), G:Cs_2CO_3 (3.70 eV), and G:CsF (3.25 eV).

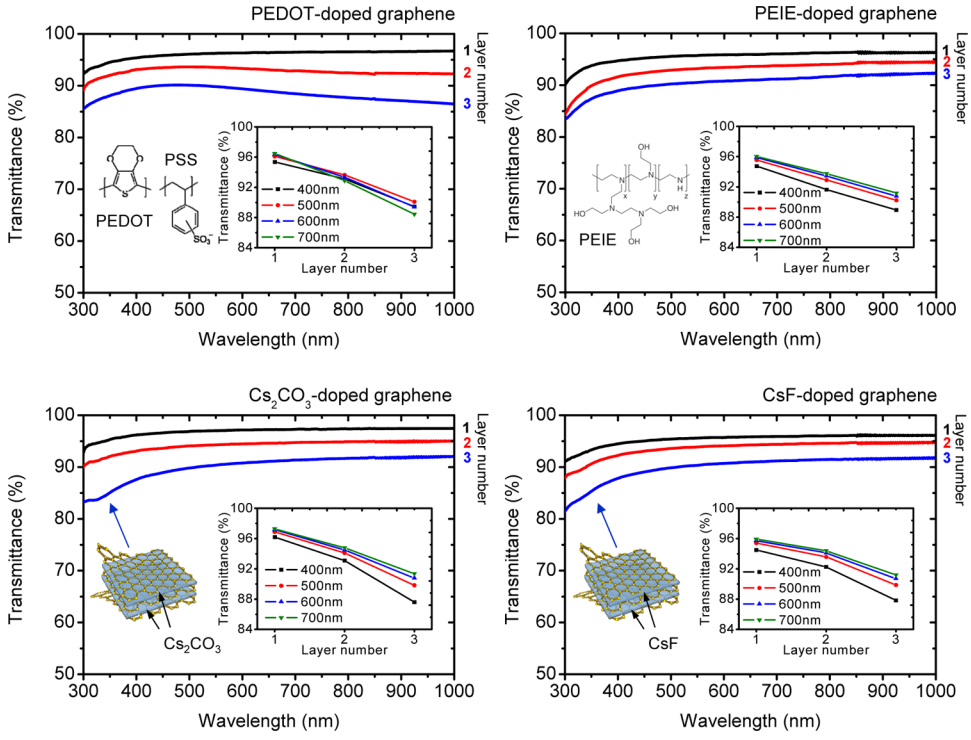

Figure 5. Transmission spectra of the doped graphene films with various layer numbers on glass substrates. The chemical structures of polymer dopants, schematic LBL structures, and the transmittance at visible wavelengths (400, 500, 600, and 700 nm) are included as insets.

consists of the commonly used poly(3-hexylthiophene)/phenyl-C61-butyric acid methyl ester (P3HT/PCBM) as the active layers. The p-type G:PEDOT was used as a transparent anode and the n-type G:CsF was applied as a transparent cathode in the BHJ OSCs of the standard and inverted structures, respectively. The device structure and energy band alignment with corresponding current density (J)−applied voltage (V) characteristics are shown in Figure 7. Similar devices with pristine graphene electrodes for comparison were also fabricated. Both doped and undoped graphene films used in the BHJ OSC device were in a trilayer configuration to reduce the sheet resistance. The detailed processing conditions are described in the Experimental Section. The PCE for devices in the standard structure is improved by approximately 60%, from 1.94 to 3.10%, by incorporating high work function G:PEDOT as an anode instead of pristine graphene. The incorporation of low work function graphene, G:CsF, into the devices in the inverted structure as the cathode enhances the PCS by approximate 97%, from 1.02 to 2.01%, as compared to that with pristine graphene. The enhancements in PCE are due to the significant improvement of open-circuit voltage (V_{oc}) and fill factor (FF). Since V_{oc} depends strongly on the work function difference between anodes and cathodes, the results verify that introducing dopant materials into graphene with our

DOI: 10.1021/acsami.5b03934
ACS Appl. Mater. Interfaces 2015, 7, 17155−17161

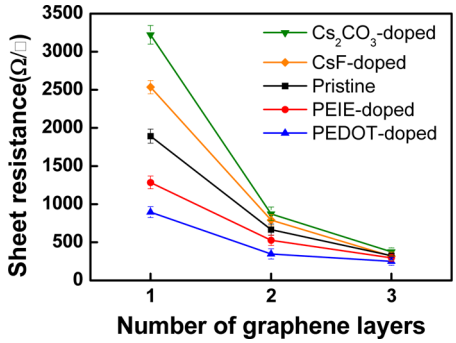

Figure 6. Sheet resistances of the doped graphene layers on glass substrates consisting of various intercalated structures.

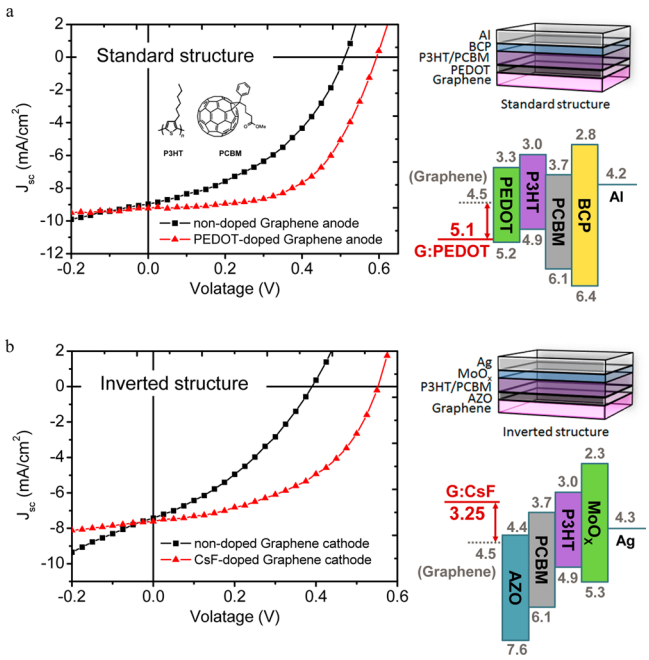

Figure 7. $J-V$ characteristics, cell architecture, and energy band diagram for BHJ-based solar cells using doped graphene as transparent electrodes in (a) standard structure of glass/G or G:PEDOT anode/PEDOT/P3HT:PCBM/BCP/Al and (b) inverted structure of glass/G or G:CsF cathode/AZO/P3HT:PCBM/MoO_x/Ag.

proposed method could modulate the work function of graphene and establish either p-type or n-type layers for desired application. This is in addition to the reduction of series resistance (R_s) observed in devices using doped graphene electrodes, which correlates well with the decrease in sheet resistance for trilayer doped graphene. In Table 1 a summary of the photovoltaic parameters derived from $J-V$ characteristics is shown, suggesting that the graphene intercalation structure obtained through our aqueous transfer process with in situ solution doping could produce graphene layers with desired work function for electrodes and gives significant improvement of V_{oc}, FF, PCE, and R_s in solar cells.

CONCLUSION

In conclusion, an aqueous transfer with concurrent doping process for graphene film has been successfully developed to efficiently dope graphene layers. Through application of this method, various doped graphene films in intercalation structures can be obtained with excellent transparency. In addition, the effective doping ratio has been carefully investigated via UPS and XPS measurements. The proposed facile strategy for doping graphene has led to a tunable work function from 3.25 to 5.10 eV, which extensively covers wide ranges of anode and cathode applications. A PCE over 3% was achieved for a device with a graphene anode, and the devices with graphene cathodes, which were rarely demonstrated, were also shown to possess a PCE of 2.01%.

EXPERIMENTAL SECTION

Aqueous Transfer with Concurrent Doping Process for Graphene. Monolayer graphene films were grown by the CVD process on copper foils as described in previous paper.[32] The graphene/copper sheets in desired sizes were placed into a graphite holder floating on ammonium persulfate etchant (Alfa Aesar, 0.2 M) in order to etch the copper. After copper foil was thoroughly removed, a blend of aqueous solution (DI water and IPA mixed in the ratio of 10:1) was substituted for the etchant with two syringe pumps, one for adding the solvent and another one for pumping out the etchant simultaneously. At the same time, the dopants, such as PEDOT:PSS (Heraeus, Clevios PH 1000), PEIE (Aldrich, 0.05 wt %), Cs_2CO_3 (CERAC, 0.05 wt %), and CsF (Alfa Aesar, 0.05 wt %), were gradually added into the aqua solvent and were incorporated into the floating graphene film by liquid phase diffusion. The doped solution was then partially rinsed before setting an arbitrary target beneath the doped graphene, ensuring the immersed target substrate is free from impurities. Finally, the aqueous solution was pumped out to lower the doped graphene onto a target substrate and the sample was dried for several minutes to remove liquid and improve the adhesion. It should be noted that the graphene stacked film intercalated with dopants can be achieved by repeating this transfer method. The quality of as-transferred graphene films was characterized by Raman spectroscopy and demonstrated flawless planarity with almost no Raman D-band as shown in Figure S1.

Fabrication of a BHJ Solar Cell. The BHJ solar cells used in this study were composed of glass/graphene or G:PEDOT/PEDOT/P3HT:PCBM/BCP/Al for the normal-structure devices with graphene layers as anode and glass/graphene or G:CsF/AZO/P3HT:PCBM/MoO_x/Ag for the inverted-structure devices with graphene layers as cathodes. The trilayer intercalated graphene sheets were transferred onto the precleaned glass substrates using the aqueous method with the in situ doping process mentioned above. For the normal devices, the PEDOT:PSS (5000 rpm for 40 s) was subsequently spun-cast onto a graphene anode and then baked in air at 120 °C for 15 min. The top surface of the graphene anode was doped with $AuCl_3$ (Aldrich, 20 mM) and the PEDOT was diluted with IPA in order to improve the

Table 1. Photovoltaic Parameters of the BHJ Solar Cell Using Pristine and Doped Graphene Trilayer Sheets as Transparent Electrodes

	electrode	work function [eV]	PCE [%]	V_{oc} [V]	J_{sc} [mA cm^{-2}]	FF [%]	R_s [Ω cm^2]
anode[a]	G:PEDOT	5.10	3.10	0.594	9.23	56.4	11.5
	G	4.50	1.94	0.510	8.97	42.4	18.5
cathode[b]	G:CsF	3.25	2.01	0.551	7.62	48.0	14.9
	G	4.50	1.02	0.390	7.43	35.1	25.6

[a]Devices using the graphene anode are in the standard structure. [b]Devices using the graphene cathode are in the inverted structure.

DOI: 10.1021/acsami.5b03934
ACS Appl. Mater. Interfaces 2015, 7, 17155−17161

surface wettability of the graphene.[34] The sol−gel AZO layers, which are prepared by the Zn precursor consisting of 0.5 M zinc acetate and monoethanolamine (MEA) in IPA with 1.35% aluminum nitrate in molar ratio, was deposited onto the graphene cathode as electron transport layers and subsequently baked at 280 °C for 10 min.[38] The following spin-cast P3HT:PCBM blend (Aldrich, 1:1 with 2.5 wt % in dichlorobenzene) was performed in a nitrogen-filled glovebox at 600 rpm for 40 s followed by 2000 rpm for 2 s. The dried film was then annealed at 150 °C for 5 min in N_2 atmosphere before being transferred into a vacuum chamber for deposition. A 20-Å BCP thin film followed by a 600-Å aluminum cathode was thermally deposited at a pressure below 10^{-5} Torr to form a 6 mm^2 graphene based BHJ solar cell in a standard structure. In a similar manner, a 15-Å MoO_x interlayer prior to the 850-Å silver anode was deposited for interfacial modification to facilitate carrier extraction in the inverted BHJ solar cell.[39,40]

Materials and Device Characterizations. The BHJ solar cells were characterized inside a MBRUAN glovebox by a Keithley 2400 source meter under AM1.5G illumination with an irradiation intensity of 100 mW cm^{-2}. The transmittance spectra of the graphene/dopant stacks were analyzed using a UV−vis−NIR spectrophotometer (Jasco V-670). The sheet resistance was measured using a four-point probe. The photoemission experiments were carried out with a Physical Electronics Phi5400 system, including an ultrahigh vacuum chamber for spectroscopic analysis with a base pressure of 10^{-10} Torr. The samples were supplied with a bias of −5 V during the valence-band UPS measurement to seclude the secondary edge for the analyzer. The photoelectrons excited by He II ($h\nu$ = 40.8 eV) sources were collected using a hemispherical analyzer with an overall resolution of 0.05 eV. The doped graphene films for photoemission experiments were transferred onto gold substrates with corresponding doping processes and then loaded into a vacuum chamber for spectroscopic analysis. High-resolution synchrotron-radiation photoemission spectroscopy was performed at the National Synchrotron Radiation Research Center (NSRRC), Hsinchu, Taiwan, R.O.C. The high-brightness photon beam was provided by the MAGM(BL08B) with photon energies in the range 300−1000 eV. The core level spectra were measured with photon energies chosen to optimize the signal-to-noise ratio.

■ ASSOCIATED CONTENT

Supporting Information

The Supporting Information is available free of charge on the ACS Publications website at DOI: 10.1021/acsami.5b03934.

Raman spectra for pristine graphene, G:PEDOT, and G:PEIE (PDF)

■ AUTHOR INFORMATION

Corresponding Authors

*E-mail: meihsinchen@mail.ndhu.edu.tw.
*E-mail: chihiwu@cc.ee.ntu.edu.tw.

Author Contributions

J.-K.C. and W.-H.L. contributed to this work equally. J.-K.C. designed and performed the doping process with data analysis; W.-H.L. developed the transfer method; J.-K.C, J.-I.T., and T.-H.C. carried out the solar cell experiments; J.-K.C., G.-K.L., and T.-W.P. performed the sample characterization and surface analysis. M.-H.C. and C.-I.W. provided the advice on and coordinated the experiments. J.-K.C. and C.-I.W. wrote the manuscript and all authors contributed equally toward improving it.

Notes

The authors declare no competing financial interest.

■ ACKNOWLEDGMENTS

The authors thank Angel Yan for informative discussions in figure demonstration. This work is supported by National Science Council of the Republic of China (NSC 101-2628-M-002-004-MY3 and NSC 102-2622-E-002-014) and the Center for Emerging Materials and Advanced Devices, National Taiwan University.

■ REFERENCES

(1) Novoselov, K. S.; Geim, A. K.; Morozov, S. V.; Jiang, D.; Zhang, Y.; Dubonos, S. V.; Grigorieva, I. V.; Firsov, A. A. Electric Field Effect in Atomically Thin Carbon Films. *Science* **2004**, *306*, 666−669.

(2) Geim, A. K.; Novoselov, K. S. The Rise of Graphene. *Nat. Mater.* **2007**, *6*, 183−191.

(3) Geim, A. K. Graphene: Status and Prospects. *Science* **2009**, *324*, 1530−1534.

(4) Bonaccorso, F.; Sun, Z.; Hasan, T.; Ferrari, A. C. Graphene Photonics and Optoelectronics. *Nat. Photonics* **2010**, *4*, 611−622.

(5) Liu, Z. K.; Li, J. H.; Sun, Z. H.; Tai, G. A.; Lau, S. P.; Yan, F. The Application of Highly Doped Single-Layer Graphene as the Top Electrodes of Semitransparent Organic Solar Cells. *ACS Nano* **2012**, *6*, 810−818.

(6) Hsu, C. L.; Lin, C. T.; Huang, J. H.; Chu, C. W.; Wei, K. H.; Li, L. J. Layer-by-Layer Graphene/TCNQ Stacked Films as Conducting Anodes for Organic Solar Cells. *ACS Nano* **2012**, *6*, 5031−5039.

(7) Liu, J.; Yin, Z.; Cao, X.; Zhao, F.; Ling, A.; Xie, L.; Fan, Q. L.; Boey, F.; Zhang, H.; Huang, W. Bulk Heterojunction Polymer Memory Devices with Reduced Graphene Oxide as Electrodes. *ACS Nano* **2010**, *4*, 3987−3992.

(8) Wu, J.; Agrawal, M.; Becerril, H. A.; Bao, Z.; Liu, Z.; Chen, Y.; Peumans, P. Organic Light-Emitting Diodes on Solution-Processed Graphene Transparent Electrodes. *ACS Nano* **2010**, *4*, 43−48.

(9) Chang, H. X.; Sun, Z. H.; Ho, K. Y. F.; Tao, X. M.; Yan, F.; Kwok, W. M.; Zheng, Z. J. A Highly Sensitive Ultraviolet Sensor Based on a Facile in Situ Solution-Grown ZnO Nanorod/Graphene Heterostructure. *Nanoscale* **2011**, *3*, 258−264.

(10) Lee, S.; Jo, G.; Kang, S. J.; Wang, G.; Choe, M.; Park, W.; Kim, D. Y.; Kahng, Y. H.; Lee, T. Enhanced Charge Injection in Pentacene Field-Effect Transistors with Graphene Electrodes. *Adv. Mater.* **2011**, *23*, 100−105.

(11) Gomez De Arco, L. G.; Zhang, Y.; Schlenker, C. W.; Ryu, K.; Thompson, M. E.; Zhou, C. W. Continuous, Highly Flexible, and Transparent Graphene Films by Chemical Vapor Deposition for Organic Photovoltaics. *ACS Nano* **2010**, *4*, 2865−2873.

(12) Wu, Y. Q.; Lin, Y. M.; Bol, A. A.; Jenkins, K. A.; Xia, F. N.; Farmer, D. B.; Zhu, Y.; Avouris, P. High-Frequency, Scaled Graphene Transistors on Diamond-Like Carbon. *Nature* **2011**, *472*, 74−78.

(13) Shi, Y. M.; Fang, W. J.; Zhang, K. K.; Zhang, W. J.; Li, L. J. Photoelectrical Response in Single-Layer Graphene Transistors. *Small* **2009**, *5*, 2005−2011.

(14) Sinitskii, A.; Tour, J. M. Lithographic Graphitic Memories. *ACS Nano* **2009**, *3*, 2760−2766.

(15) Dong, X. C.; Shi, Y. M.; Huang, W.; Chen, P.; Li, L. J. Electrical Detection of DNA Hybridization with Single-Base Specificity Using Transistors Based on CVD-Grown Graphene Sheets. *Adv. Mater.* **2010**, *22*, 1649−1653.

(16) Pirkle, A.; Chan, J.; Venugopal, A.; Hinojos, D.; Magnuson, C. W.; McDonnell, S.; Colombo, L.; Vogel, E. M.; Ruoff, R. S.; Wallace, R. M. The Effect of Chemical Residues on the Physical and Electrical Properties of Chemical Vapor Deposited Graphene Transferred to SiO_2. *Appl. Phys. Lett.* **2011**, *99*, 122108.

(17) Lee, Y. Y.; Tu, K. H.; Yu, C. C.; Li, S. S.; Hwang, J. Y.; Lin, C. C.; Chen, K. H.; Chen, L. C.; Chen, H. L.; Chen, C. W. Top Laminated Graphene Electrode in a Semitransparent Polymer Solar Cell by Simultaneous Thermal Annealing/Releasing Method. *ACS Nano* **2011**, *5*, 6564−6570.

(18) Cheng, Z.; Zhou, Q.; Wang, C.; Li, Q.; Wang, C.; Fang, Y. Toward Intrinsic Graphene Surfaces: A Systematic Study on Thermal

DOI: 10.1021/acsami.5b03934
ACS Appl. Mater. Interfaces 2015, 7, 17155−17161

Annealing and Wet-Chemical Treatment of SiO2-Supported Graphene Devices. *Nano Lett.* **2011**, *11*, 767−771.
(19) Wang, Y.; Tong, S. W.; Xu, X. F.; Özyilmaz, B.; Loh, K. P. Interface Engineering of Layer-by-Layer Stacked Graphene Anodes for High-Performance Organic Solar Cells. *Adv. Mater.* **2011**, *23*, 1514−1518.
(20) Yan, Z.; Sun, Z.; Lu, W.; Yao, J.; Zhu, Y.; Tour, J. M. Controlled Modulation of Electronic Properties of Graphene by Self-Assembled Monolayers on SiO2 Substrates. *ACS Nano* **2011**, *5*, 1535−1540.
(21) Lee, B.; Chen, Y.; Duerr, F.; Mastrogiovanni, D.; Garfunkel, E.; Andrei, E. Y.; Podzorov, V. Modification of Electronic Properties of Graphene with Self-Assembled Monolayers. *Nano Lett.* **2010**, *10*, 2427−2432.
(22) Giovannetti, G.; Khomyakov, P. A.; Brocks, G.; Karpan, V. M.; Van den Brink, J.; Kelly, P. J. Doping Graphene with Metal Contacts. *Phys. Rev. Lett.* **2008**, *101*, 026803.
(23) Shi, Y.; Kim, K. K.; Reina, A.; Hofmann, M.; Li, L. J.; Kong, J. Work Function Engineering of Graphene Electrode via Chemical Doping. *ACS Nano* **2010**, *4*, 2689−2694.
(24) Kim, K. K.; Bae, J. J.; Park, H. K.; Kim, S. M.; Geng, H. Z.; Park, K. A.; Shin, H. J.; Yoon, S. M.; Benayad, A.; Choi, J. Y.; Lee, Y. H. Fermi Level Engineering of Single-Walled Carbon Nanotubes by AuCl3 Doping. *J. Am. Chem. Soc.* **2008**, *130*, 12757−12761.
(25) Liu, Z. K.; Li, J. H.; Yan, F. Package-Free Flexible Organic Solar Cells with Graphene Top Electrodes. *Adv. Mater.* **2013**, *25*, 4296−4301.
(26) Han, T. H.; Lee, Y.; Choi, M. R.; Woo, S. H.; Bae, S. H.; Hong, B. H.; Ahn, J. H.; Lee, T. W. Extremely Efficient Flexible Organic Light-Emitting Diodes with Modified Graphene Anode. *Nat. Photonics* **2012**, *6*, 105−110.
(27) Kim, H.; Bae, S. H.; Han, T. H.; Lim, K. G.; Ahn, J. H.; Lee, T. W. Organic Solar Cells Using CVD-Grown Graphene Electrodes. *Nanotechnology* **2014**, *25*, 014012.
(28) Cho, H.; Kim, S. D.; Han, T. H.; Song, I.; Byun, J. W.; Kim, Y. H.; Kwon, S.; Bae, S. H.; Choi, H. C.; Ahn, J. H.; Lee, T. W. Improvement of Work Function and Hole Injection Efficiency of Graphene Anode Using CHF3 Plasma Treatment. *2D Mater.* **2015**, *2*, 014002.
(29) Lu, A. Y.; Wei, S. Y.; Wu, C. Y.; Hernandez, Y.; Chen, T. Y.; Liu, T. H.; Pao, C. W.; Chen, F. R.; Li, L. J.; Juang, Z. Y. Decoupling of CVD Graphene by Controlled Oxidation of Recrystallized Cu. *RSC Adv.* **2012**, *2*, 3008−3013.
(30) Song, L.; Ci, L. J.; Gao, W.; Ajayan, P. M. Transfer Printing of Graphene Using Gold Film. *ACS Nano* **2009**, *3*, 1353−1356.
(31) Zhang, D.; Xie, F.; Lin, P.; Choy, W. C. H. Al-TiO2 Composite-Modified Single-Layer Graphene as an Efficient Transparent Cathode for Organic Solar Cells. *ACS Nano* **2013**, *7*, 1740−1747.
(32) Lin, W. H.; Chen, T. H.; Chang, J. K.; Taur, J. I.; Lo, Y. Y.; Lee, W. L.; Chang, C. S.; Su, W. B.; Wu, C. I. A Direct and Polymer-Free Method for Transferring Graphene Grown by Chemical Vapor Deposition to Any Substrate. *ACS Nano* **2014**, *8*, 1784−1791.
(33) Zhou, Y.; Fuentes-Hernandez, C.; Shim, J.; Meyer, J.; Giordano, A. J.; Li, H.; Winget, P.; Papadopoulos, T.; Cheun, H.; Kim, J.; Fenoll, M.; Dindar, A.; Haske, W.; Najafabadi, E.; Khan, T. M.; Sojoudi, H.; Barlow, S.; Graham, S.; Brédas, J.-L.; Marder, S. R.; Kahn, A.; Kippelen, B. A Universal Method To Produce Low-Work Function Electrodes for Organic Electronics. *Science* **2012**, *336*, 327−332.
(34) Park, H.; Shi, Y.; Kong, J. Application of Solvent Modified PEDOT:PSS to Graphene Electrodes in Organic Solar Cells. *Nanoscale* **2013**, *5*, 8934−8939.
(35) Wang, Y.; Chen, X.; Zhong, Y.; Zhu, F.; Loh, K. P. Large Area, Continuous, Few-Layered Graphene as Anodes in Organic Photovoltaic Devices. *Appl. Phys. Lett.* **2009**, *95*, 063302.
(36) Luo, Z. Q.; Shang, J. Z.; Lim, S. H.; Li, D. H.; Xiong, Q. H.; Shen, Z. X.; Lin, J. Y.; Yu, T. Modulating the Electronic Structures of Graphene by Controllable Hydrogenation. *Appl. Phys. Lett.* **2010**, *97*, 233111.
(37) Ha, Y. H.; Nikolov, N.; Pollack, S.; Mastrangelo, J.; Martin, B.; Shashidhar, R. Towards a Transparent, Highly Conductive Poly(3,4-ethylenedioxythiophene). *Adv. Funct. Mater.* **2004**, *14*, 615−622.
(38) Tsai, S. H.; Ho, S. T.; Jhuo, H. J.; Ho, C. R.; Chen, S. A.; He, J. H. Toward High Efficiency of Inverted Organic Solar Cells: Concurrent Improvement in Optical and Electrical Properties of Electron Transport Layers. *Appl. Phys. Lett.* **2013**, *102*, 253111.
(39) Bernede, J. C.; Houari, S.; Nguyen, D.; Jouan, P. Y.; Khelil, A.; Mokrani, A.; Cattin, L.; Predeep, P. XPS Study of the Band Alignment at ITO/Oxide (n-Type MoO_3 or p-Type NiO) Interface. *Phys. Status Solidi A* **2012**, *209*, 1291−1297.
(40) Du, Y.; Peng, H.; Mao, H.; Jin, K.; Wang, H.; Li, F.; Gao, X. Y.; Chen, W.; Wu, T. Evolution of the $SrTiO_3/MoO_3$ Interface Eectronic Structure: An in situ Photoelectron Spectroscopy Study. *ACS Appl. Mater. Interfaces* **2015**, *7*, 11309−11314.

DOI: 10.1021/acsami.5b03934
ACS Appl. Mater. Interfaces 2015, 7, 17155−17161